

# Hydraulic modelling of instabilities on half-round circular weirs at three scales

Hubert Chanson 

The University of Queensland, School of Civil Engineering, Brisbane QLD 4072, Australia

## ABSTRACT

The half-round circular weir is a seminal design that has been extensively studied for relatively small discharges. Recent experimental works reported a number of instabilities, nonlinearities and hysteresis at medium to large discharges. Detailed physical investigations with a half-round circular weir were undertaken in the absence of ventilation at three geometric scales for an identical relative height and breadth. Three basic flow patterns were observed. The flow conditions for the change in flow patterns did not scale according to a Froude similitude. Cyclic flow patterns were observed for a range of constant discharges at all scales, and these nonlinearities were caused by the lack of ventilation. The quantitative measurements also indicated some hysteresis, with different data obtained whether for increasing or decreasing discharge experimental conditions, underlying the limitations of the Froude similitude.

## ARTICLE HISTORY

Received 26 March 2025  
Accepted 6 July 2025  
Open for discussion until  
1 February 2026

## KEYWORDS

Half-round spillway crest;  
hydraulic structures;  
instabilities; nonlinearities;  
physical modelling; scale  
effects

## 1. Introduction

At a control structure for free-surface flows, the shape of the passage controls the discharge capacity. Among the many crest designs (Ackers et al., 1978; Bos, 1976), the half-round circular weir (Figure 1) is a seminal crest design that has been extensively studied during the last eight decades for relatively small discharges, i.e.  $d_c/r < 1$  to 1.5 with  $d_c$  being the critical depth and  $r$  the radius of curvature (Chanson & Montes, 1998; Fawer, 1937; Matthew, 1963; Ramamurthy & Vo, 1993). Recently, a number of experimental studies investigated medium to large discharges (i.e.  $1.5 < d_c/r < 10$ ) and the results indicated a number of large discrepancies associated with the hysteresis above circular weirs in the absence of ventilation (Chanson, 2020; Tullis et al., 2019). That is, the relationship between the overflow discharge and upstream above the crest differed depending on whether the flow conditions corresponded to an increasing discharge, e.g. the rising limb of a flood hydrograph, or to a decreasing discharge. Such hydrodynamic instabilities have adverse effects on the upscaling of physical and numerical modelling, including the implicit limitations of tests conducted over short periods. Further, questions may be asked about the validity of extrapolated results (Anderson & Tullis, 2018; MWSDB, 1980).

In terms of instability, nonlinearity and fluctuation of flow characteristics over weirs, there is some well-respected literature on fluttering instabilities of thin nappes (e.g. Caspersen, 1993; Pariset, 1955; Petrikat,

1958, 1978) and on cross-waves (e.g. Hager, 1992; Ippen & Harleman, 1956). In the context of nappe instabilities above half-round circular weirs, the bibliography is very limited. It is the aim of this contribution to provide a detailed methodology for the sound characterization of half-round circular weir overflow, encompassing flow instabilities and hysteresis. The results enable some reflections on the intricacy of the experimental methodology and the challenges of upscaling.

## 2. Dimensional analysis and similitude

### 2.1. Basic considerations

Hydraulic models are typically utilized during the design stages and operational life of hydraulic structures to optimize the final design and the safe operation during both minor and major flood events (Novak & Cabelka, 1981). The model study aims to provide a reliable prediction of prototype performances, and this is achieved by performing model experiments under controlled flow and boundary conditions. In physical and numerical models, the flow properties must be similar to those at full-scale, in terms of geometric, kinematic and dynamic similarity (Foss et al., 2007; Liggett, 1994).

The modelling approach must be developed based upon the fundamental principles of dimensional analysis and similitude (Bertrand, 1878; Vaschy, 1892). Considering a half-round circular weir in a rectangular channel in the absence of ventilation (Figure 2), a basic dimensional analysis shows a large number of relevant



**Figure 1.** Half-round circular crested weir at Barrage de Pont Ruffier (France) on 2 August 2024.

parameters. A simplified dimensional analysis yields a series of steady flow properties as functions of key relevant parameters identified for the discharge performances of a half-round circular weir:

$$Q, d_{crest}, \dots = F_1(H_1, P, r, B, k_s, \theta, g, \rho, \mu, \sigma) \quad (1)$$

where  $Q$  is the discharge,  $d_{crest}$  is the water depth above the weir crest,  $H_1$  is the upstream total head,  $P$  is the weir height,  $r$  is the radius of curvature,  $B$  is the channel breadth,  $k_s$  is the equivalent sand roughness height of the weir crest,  $\theta$  is the channel slope,  $g$  is the gravity acceleration,  $\rho$  is the water density,  $\mu$  is the dynamic viscosity of water, and  $\sigma$  is the surface tension. In Equation (1), the dimensions of the independent variables can be grouped into three categories, i.e. mass (M), length (L) and time (T). Based upon the  $\Pi$ -Vaschy-Buckingham theorem (Buckingham, 1914; Vaschy, 1892), Equation (1) may be rewritten in dimensionless terms as:

$$C_D, \frac{d_{crest}}{r}, \dots = F_2\left(\frac{H_1 - P}{r}, \frac{P}{r}, \frac{B}{r}, \frac{k_s}{r}, \theta, Re, Mo\right) \quad (2)$$

with  $C_D$  the dimensionless discharge coefficient,  $Re$  the Reynolds number and  $Mo$  the Morton number defined respectively as:

$$Re = \rho \times \frac{V \times d}{\mu} \quad (3)$$

$$Mo = \frac{g \times \mu^4}{\rho \times \sigma^3} \quad (4)$$

In the present study of free-surface flows, the gravity effects were important and a Froude similarity was applied, i.e. the Froude number was the same in model and prototype. Further, the same fluid, i.e. air and water, were used in laboratory and prototype, i.e.

$Mo = \text{constant}$ . Thus, the Weber number became irrelevant in the hydraulic modelling of half-round circular weirs, when the Froude, Reynolds and Morton numbers are retained in Equation (2) (Chanson, 1997, 2004; Kobus, 1984).

In addition, the channel was horizontal ( $\theta = 0$ ), the weir crest was very smooth (i.e.  $k_s \approx 0$ ), and the ratio  $B/r$  of channel breadth to radius of curvature was kept constant, with the same value  $B/r = 40$ . More, the characteristics of half-round circular weirs were investigated at three physical scales for an identical dimensionless ratio  $P/r = 25$ . Thus, the dimensionless Equation (2) may be simplified for a steady flow above a half-round circular weir:

$$C_D, \frac{d_{crest}}{r}, \dots = F_3\left(\frac{H_1 - P}{r}, Re\right) \quad (5)$$

A combined Froude and Morton similitude was applied in the current study and the Reynolds number, in Equation (5), accounted for any potential scale effect linked to capillary and viscous processes.

### 3. Experimental facility and instrumentation

#### 3.1. Presentation

The experiments were conducted in the Hydraulics Laboratory at the University of Queensland, Australia. Three weirs were used with identical dimensionless height  $P/r = 25$  and breadth  $B/r = 40$ , but different radius of curvature  $r$  (Table 1). In all the facilities, the channel invert was horizontal, it was made of PVC and the sidewalls were in glass. In each facility, the water was supplied by an upstream intake water tank equipped with baffles and flow straighteners, leading the water

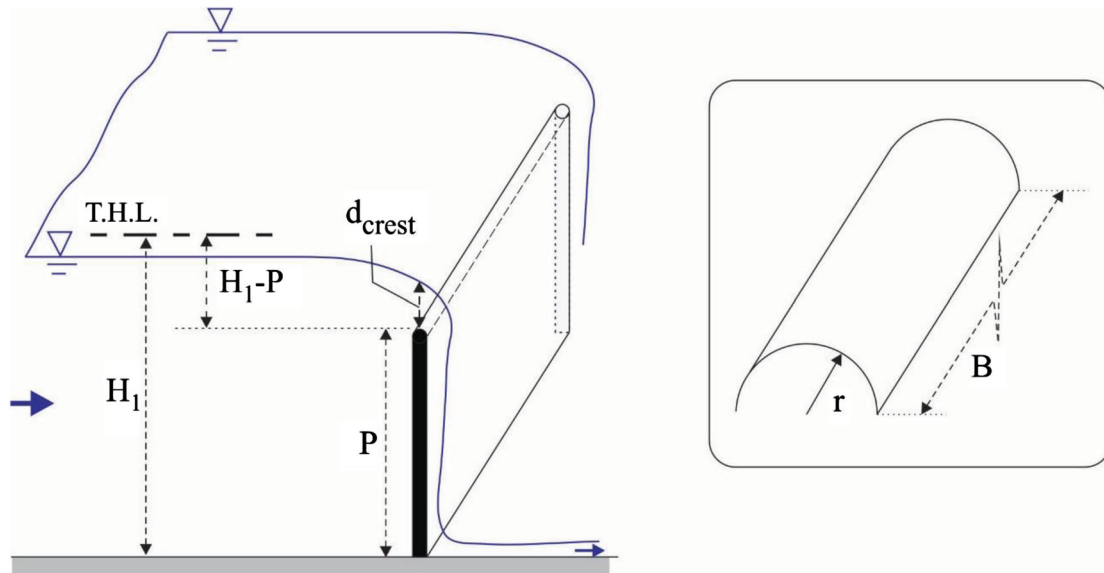


**Figure 2.** Definition sketch of half-round circular weir. Inset (right): details of the half-round circular crest.

**Table 1.** Experimental flow conditions for a half-round circular weir study at three scales with  $P/r = 25$  and  $B/r = 40$ .

Configuration	$\theta$	$x_1$ (m)	$P$ (m)	$r$ (m)	$B$ (m)	$P/r$	$B/r$	$d_1$ (m)	$Q$ ( $\text{m}^3 \text{s}^{-1}$ )	Re	Comments
Type I	0	1.34	0.250	0.010	0.40	25	40	0.2555–0.374	$3 \times 10^{-5}$ to $4 \times 10^{-2}$	$2.98 \times 10^3$ to $3.9 \times 10^5$	Unventilated. Incl. experiments by Chanson (2020).
Type II	0	1.68	0.3125	0.0125	0.50	25	40	0.322–0.447	$3.6 \times 10^{-3}$ to $6 \times 10^{-2}$	$2.9 \times 10^4$ to $4.7 \times 10^5$	Unventilated.
Type III	0	2.93	0.4375	0.0175	0.70	25	40	0.453–0.496	$2.5 \times 10^{-4}$ to $4.7 \times 10^{-2}$	$1.4 \times 10^4$ to $1.2 \times 10^5$	Unventilated.

Notes:  $B$ , channel breadth;  $d_1$ , upstream water depth;  $P$ , weir height;  $Q$ , water discharge; Re, Reynolds number defined in terms of the hydraulic diameter and velocity;  $r$ , radius of curvature;  $x_1$ , longitudinal location of the circular weir measured from the upstream end of the glass sidewalled flume;  $\theta$ , angle between channel invert and horizontal. Columns 9, 10 and 11 list the range of investigated flow conditions.

to the flume through a smooth three-dimensional convergent intake (Chanson, 2025). The flow rate provided to the intake structure was supplied by a water reticulation system equipped with a constant-head reservoir. The combination of a constant head water system and advanced intake structure ensured a constant inflow with smooth inflow conditions to the upstream end of the flume. A free overfall ended the flume.

The half-round circular weir Type I was a 0.250 m high weir, 0.010 m radius and a 0.020 m thick vertical wall, i.e.  $P = 0.250$  m,  $r = 0.010$  m, with wall thickness  $2 \times r$  (Figure 2). It was tested in a 3 m long 0.4 m wide flume, i.e.  $B = 0.4$  m, previously used by Chanson (2020). A 12 m long and 0.5 m wide flume was used with the half-round circular weir Type II ( $r = 0.0125$  m). The water discharge was measured by an orifice meter installed in the pipe of the reticulation system and the error of the flow rate was less than 2%. A 19 m long 0.7 m wide flume was used with half-round circular weir Type III ( $r = 0.0175$  m). The flow rate provided to the intake tank was measured by a magneto flow meter with an accuracy of  $10^{-5} \text{ m}^3 \text{ s}^{-1}$ .

In all flumes, the water depths were measured with rail-mounted pointer gauges as well as using graduated rulers through the glass sidewalls. Further observations were taken with a digital camera Sony<sup>TM</sup> DSC-RX100VA (Tokyo, Japan) recording movies at

25 fps and 100 fps, an Apple<sup>TM</sup> iPhone XI, (Cupertino CAL, USA) and a dSLR camera Pentax<sup>TM</sup> K-3iii (Tokyo, Japan). The dSLR camera was equipped with professional-grade prime lenses, which produced images with negligible degree of barrel distortion.

### 3.2. Half-round circular weir configurations

All the circular weirs were a half-round circular profile installed in the flumes. The weir profiles were designed based upon the half-round weir geometry proposed by Tullis et al. (2018) and discussed by Tullis et al. (2019). The weir dimensions are listed in Table 1. In the present study, the weirs were machined out of PVC with an accuracy of  $\pm 0.2$  mm, except for half-round circular weir Type II for which the downstream face of the weir was covered by thin marine plywood to achieve a weir thickness equal to  $2 \times r$ . For all the experiments, the weirs were installed perpendicular to the flow direction, sealed with silicone on both sides and bottom, and two buttresses were installed on the downstream side to support the pressure force acting on the weir. The nappe was unventilated.

The half-round circular weir Types II and III were respectively the 1.25:1 and 1.75:1 upscaled versions of half-round circular weir Type I.

### 3.3. Experimental flow conditions and procedure

The experiments were performed across a very wide range of discharges and Reynolds numbers (Table 1). Most experimental datasets covered a range of flow rates spanning over two orders of magnitude. For all experiments, the tailwater conditions were uncontrolled. Following the original work of Chanson (2020), all the experiments were repeated with either increasing or decreasing discharges. When an experiment was conducted with increasing discharges, the discharge was gently increased (by less than 10%). The readings were then performed after 3 min of flow establishment, and the data are presented accordingly. Once the measurements were completed, the process was then repeated with a larger flow rate. A similar procedure was applied with decreasing discharge experiments.

The readings were typically performed over 3 min of readings. When some instabilities were observed, e.g. linked to nappe detachment or reattachment, a longer observation period was automatically used. These encompassed observations for 10, 30 and 60 min to document the occurrence of any nonlinear flow instabilities. During cyclic flow conditions observed for a constant discharge (see below), with the flow features shifting between markedly different flow patterns, the observations were conducted at regular intervals across numerous cycles, for 10 to 60 min.

Finally, a number of experimental observations were repeated independently by five people for different flow conditions, to check the accuracy and repeatability of the experimental procedure and of the datasets. The experimentalists included a second-year undergraduate student, two fourth-year undergraduate students, a graduate student, and a senior academic (i.e. the author himself). Furthermore, the author himself performed physical measurements with all circular weir types (Table 1).

## 4. Basic flow patterns

For the three weirs, three basic flow patterns were observed for the ranges of investigated flow rates (Table 1). These were an attached nappe at low flow rates, a detached nappe with an air cavity beneath for intermediate discharges, and a reattached nappe at large flow rates. The flow patterns are illustrated in Figure 3. The flow conditions for the change in flow patterns are reported in Table 2. The data showed that the changes in flow patterns occurred at markedly different dimensionless discharge  $d_c/r$  (Table 2). It is acknowledged that, although the transition with decreasing discharges was closer between three configurations, the differences between the half-round circular weir Types I, II and III suggested that a simplistic Froude similarity was insufficient to represent the complicated nonlinear processes observed physically, including transients. The

finding was consistent with previous results (Anderson & Tullis, 2018; MWSDB, 1980).

At low discharges, the nappe attached to the crest and to the downstream weir wall. Above the crest, the streamlines presented a very strong curvature and no separation was observed. This flow pattern is illustrated in Figure 3a (left) and in the video movie CIMG5661.mov (see Appendix A and the online supplemental data). The dominant feature was the smooth flow around the weir, and the marked streamline curvature around the half-round profile as the flow was accelerated. For some narrow ranges of flow rates, some incomplete nappe detachment could be observed. These were best observed with the larger weirs Types II and III. Some thin, often elongated air cavities developed across section(s) of the weir, and the detached nappe reattached the weir's vertical wall before the weir toe. Figure 4 presents an illustration.

For a range of intermediate flows, the nappe was detached and a marked air cavity formed below the full breadth of the channel, with a pool of recirculating water underneath (Figure 3a (middle)). At the impingement of the lower nappe with the pool of recirculating water, some strong air entrapment was observed, similar to air bubble entrainment at plunging jets (Bertola et al., 2018; Bin, 1993; Brattberg & Chanson, 1998). Some entrapped air recirculated back into the cavity, while other amounts of air were entrained and advected into the downstream flow. In the upper range of such flow conditions, a cyclic behaviour in changes in nappe flow patterns was observed, from fully opened air cavity, to partially opened cavity and sometimes to reattached nappe (next section). The cyclic nappe behaviour was directly linked to the lack of ventilation. For a constant flow rate, the observation showed fast fluctuations super-imposed on slow fluctuations.

For large flows, the air cavity disappeared and the nappe reattached, although the streamline curvature above the crest was moderate. Some flow separation was observed with dye injection and a recirculation zone was observed beneath the overflowing nappe. The flow pattern is seen in Figure 3a (right).

## 5. Cyclic cavity flow patterns

For some ranges of intermediate flow rates, long-duration observations with a constant discharge showed the occurrence of nonlinear behaviour with some cyclic pattern between nappe reattachment and nappe detachment for a constant water discharge. The cyclic pattern was linked to the lack of ventilation. Physically, when the nappe was detached, the air entrainment at the lower nappe impingement exceeded the air resupply into the air cavity. In turn, the total air mass in the cavity decreased and the air pressure became sub-atmospheric. Gradually, the air cavity size diminished, while the sub-pressure force acting on the lower

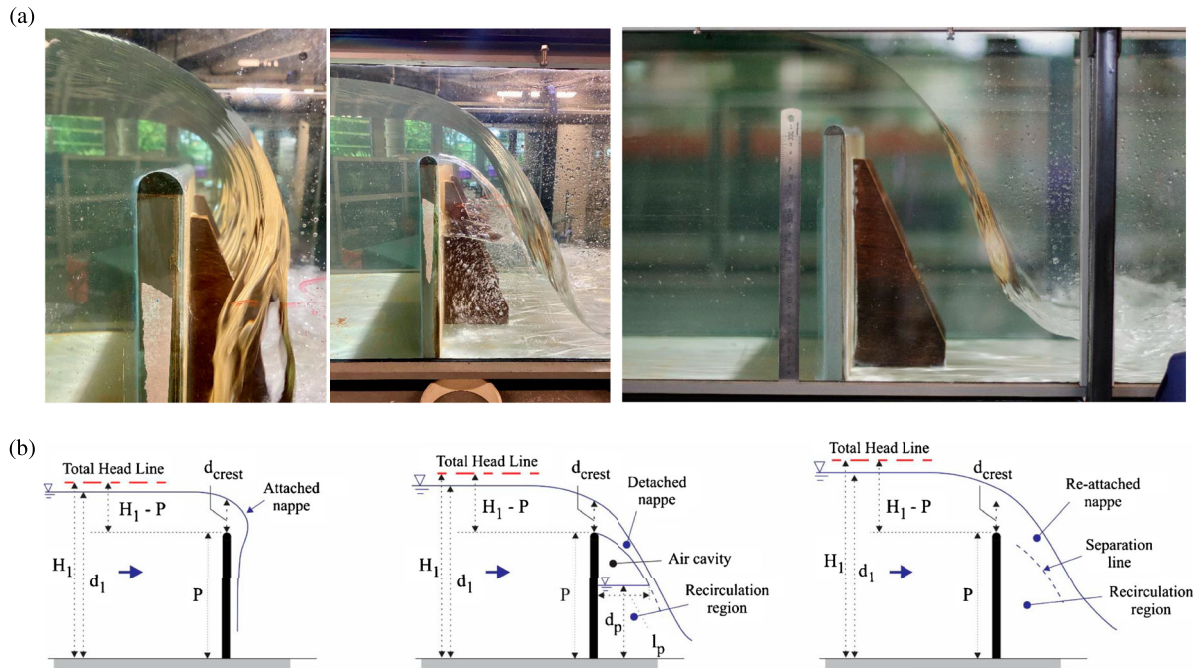


**Figure 3.** Overflow experiments on half-round circular weir: flow direction from left to right, experiments with increasing flow rate. (a) Experiments with Circular weir Type II - From left to right: attached nappe for  $d_c/r = 5.4$ ; detached nappe for  $d_c/r = 6.7$ ; re-attached nappe for  $d_c/r = 8.8$ . (b) Definition sketch of the three main flow regimes.

**Table 2.** Flow conditions for different flow regimes above a half-round circular weir with  $P/r = 25$  and  $B/r = 40$ .

Configuration	$r$ (m)	$B/r$	$P/r$	Experiment type	Attached nappe	Detached nappe	Reattached nappe <sup>(1)</sup>	Comments
Type I	0.010	40	25	Increasing discharge	$d_c/r < 5.25$	$5.25 < d_c/r < 7.25$	$d_c/r > 7.25$	Unventilated
				Decreasing discharge	$d_c/r < 1.25$ to $1.75$	$1.25$ to $1.75 < d_c/r < 6.75$	$d_c/r > 6.75$	
Type II	0.0125	40	25	Increasing discharge	$d_c/r < 5.9$	$5.9 < d_c/r < 7.4$	$d_c/r > 7.4$	Unventilated
				Decreasing discharge	$d_c/r < 1.7$ to $5.4$	$1.7$ to $5.4 < d_c/r < 7.0$	$d_c/r > 7.0$	
Type III	0.0175	40	25	Increasing discharge	$d_c/r < 1.5$	$2 < d_c/r$	N/A	Unventilated
				Decreasing discharge	$d_c/r < 1.5$	$1.5 < d_c/r$	N/A	

Notes:  $B$ , channel breadth;  $d_c$ , critical flow depth;  $P$ , weir height;  $r$ , radius of curvature; <sup>(1)</sup>, for large discharges; (N/A), not applicable.

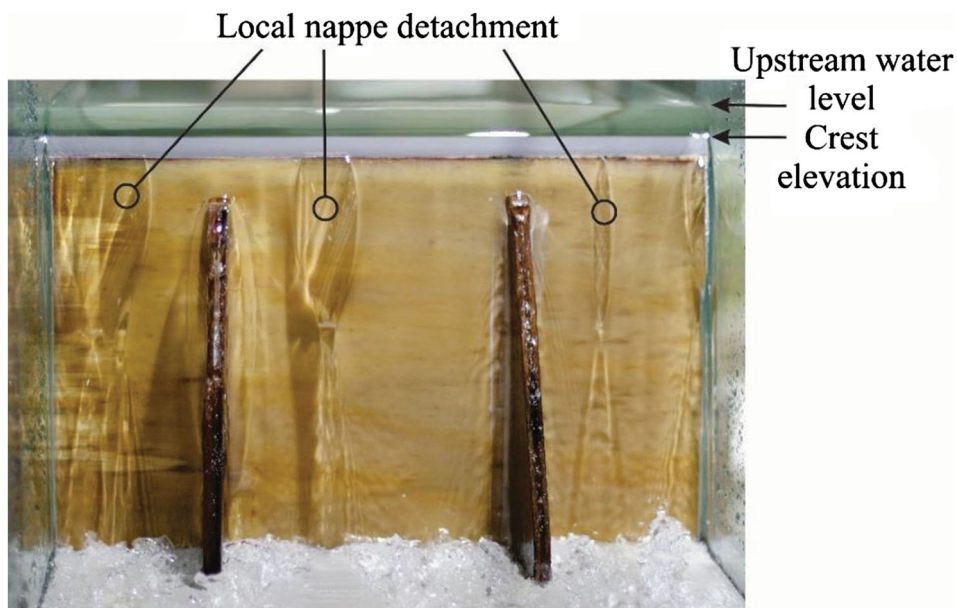


**Figure 4.** Incomplete nappe detachment at half-round circular weir looking upstream: flow conditions:  $d_c/r = 1.81$ , experiment with decreasing flow rate, half-round circular weir Type II.

**Table 3.** Flow conditions for long duration cyclic cavity flow patterns, while the discharge was kept constant, above a half-round circular weir with  $P/r = 25$  and  $B/r = 40$ .

Configuration	$r$ (m)	$B/r$	$P/r$	Experiment type	Cyclic pattern flow conditions	Comments
Type I	0.010	40	25		$5.25 < d_c/r < 5.5$	Partial cavity collapse
					$6.25 < d_c/r < 7.0$	Partial cavity collapse
					$7.0 < d_c/r < 7.75$	Complete cavity closure
Type II	0.0125	40	25	Increasing discharge	$5.9 < d_c/r < 6.8$	Partial cavity collapse
					$6.8 < d_c/r < 7.0$	Complete cavity closure
				Decreasing discharge	$3.0 < d_c/r < 6.2$	Partial cavity collapse
					$6.2 < d_c/r < 6.9$	Complete cavity closure

Notes:  $B$ , channel breadth;  $d_c$ , critical flow depth;  $P$ , weir height;  $r$ , radius of curvature.

nappe forced an inward curvature of the lower nappe which is a streamline. The overflow streamline curvature became marked and the fluid over the half-round circular crest became more accelerated downstream of the crest. With time, the air cavity disappeared and the nappe became attached without air cavity. The attached nappe was relatively unstable. Once air could enter between the wall and the water, the nappe would quasi-instantaneously detach and the air cavity formed. Air intrusion between the water and boundaries was often seen next to the sidewalls at the weir toe. As the attached nappe was accelerated by a combination of gravity and suction pressure actions, the overflowing nappe contracted both radially and transversally. The interface between the nappe and sidewalls became very thin at the weir toe, and some form of instabilities, next to sidewalls, could allow air beneath the nappe.

In most cases, the cyclic behaviour took place between detached nappe with a large air cavity and partially-attached nappe with a very small air cavity. In the most extreme cases, the flow patterns alternated between an attached nappe, a fully-detached nappe and a partially-attached nappe with a very small air cavity. The flow conditions corresponding to marked cyclic patterns, while the discharge was kept constant, are summarized in Table 3. The video movies IMG\_3223.mov and IMG\_3227.mov (Appendix A and the online supplemental data) show two different views of the overflow pattern for  $d_c/r = 6.66$  with half-round circular weir Type II during a cyclic behaviour. In each movie, the air cavity slowly shrank, before sudden nappe detachment towards the end of the movies. The movie IMG\_3223.mov (Appendix A) shows a view from downstream, looking upstream. In the first part of the movie, the lower nappe impingement perimeter is seen to fluctuate with large transverse variations and about three to four transverse wave lengths. The air cavity disappears at about 40 s, while nappe detachment takes place at about 69 s into the movie. The movie IMG\_3227.mov (Appendix A) presents a side-view of the same experiment. The air cavity closure starts to take place at about 71 s, and the nappe detaches completely at about 83 s into the movie.

Visual, photographic and cinematographic observations showed that the air cavity opening was very rapid (IMG\_3223.mov and IMG\_3227.mov, Appendix

A). The cavity opening and expansion lasted less than 1 s and this rapid transient was violent, sometimes accompanied by some loud low-frequency noise that would be heard from a distance. The initial transition would be followed by a period of slower cavity expansion, which could last more than 10–20 s. Following the air cavity expansion process, the filling of the air cavity was a much slower process, lasting several minutes. The cavity filling was caused by the net air entrapment at the plunge point of the lower nappe into the pool of recirculating waters, seen in Figure 3a (middle). Large transverse fluctuations of the lower nappe impingement perimeter were observed, as illustrated in the movie IMG\_3223.mov (Appendix A). During the cyclic conditions, the cyclic flow patterns were associated with changes in the air cavity properties (height, length, volume) as well as changes in the water depth  $d_{crest}$  at the weir crest, upstream water depth  $d_1$  and downstream depth  $d_2$  (Chanson & Memory, 2022).

A key feature of the nonlinear behaviour was the major change in streamline pattern over the weir crest during long-duration tests, as illustrated in the movie IMG\_3227.mov (Appendix A). For an attached nappe, the streamline curvature was characteristically marked at and immediately downstream of the weir crest. The radius of curvature of streamlines was slightly larger than the crest radius. With the attached nappe, the upstream water surface elevation was the lowest and the discharge coefficient was the largest, as predicted by the irrotational flow theory (Castro-Orgaz & Hager, 2017; Chanson, 2013; Vallentine, 1969), whereby the dimensionless discharge coefficient  $C_D$  is defined as:

$$C_D \times \sqrt{g \times \left( \frac{2}{3} \times (H_1 - P) \right)^3} = \frac{Q}{B} \quad (6)$$

For the same discharge, the fully-detached nappe was associated with the flattest streamlines at the weir crest, the largest upstream water elevation and the smallest discharge coefficient. The effects on the head-discharge relationship are illustrated in Figure 5. Figure 5 presents the instantaneous relationship between the dimensionless upstream head and dimensionless discharge; the data were derived from high-shutter speed dSLR photographs.

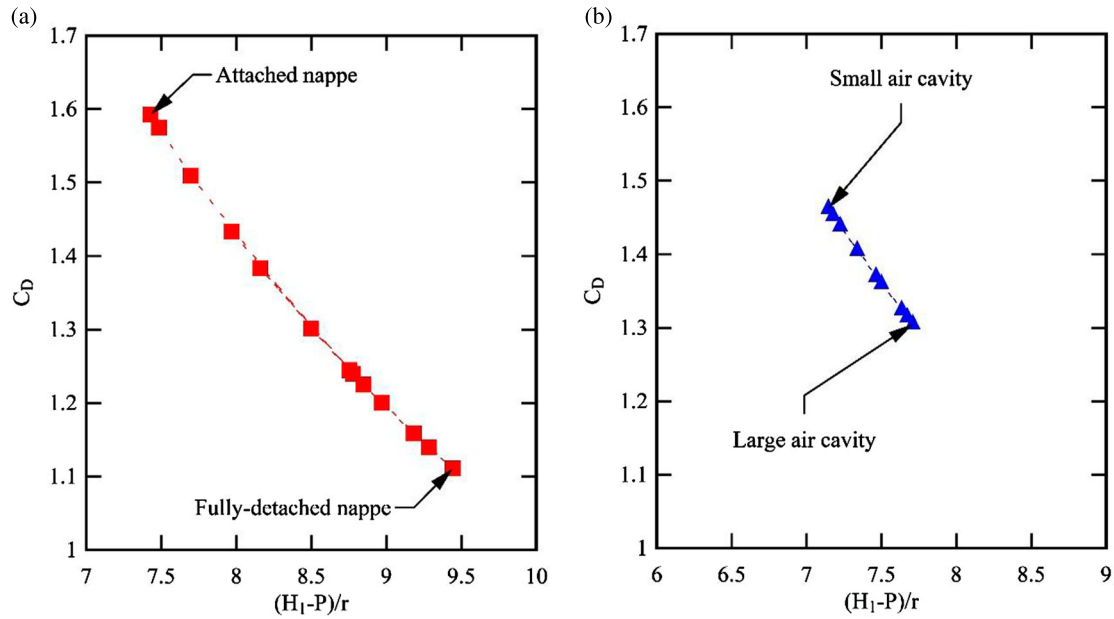


**Figure 5.** Dimensionless head-discharge relationship during a cyclic cavity flow pattern, while the discharge was kept constant: (a) complete cyclic pattern from attached to fully-detached nappe for  $d_c/r = 6.75$ , time series duration over 1000 s, Type II; (b) cyclic pattern between small and large air cavity  $d_c/r = 6.14$ , time series duration over 700 s, Type II. Both graphs use the same scales.

For completeness, Phillips et al. (2024) reported a similar cyclic flow pattern at a large nonlinear weir model with half-round crest in the absence of ventilation. For  $d_c/r \approx 4$ , unstable partially aerated nappe was reported with transverse instabilities and large dynamic pressure variations on the downstream wall face. More, large negative pressure under the nappe were observed for  $3.5 < d_c/r < 4$  (Phillips et al., 2024).

### 5.1. Commentary

The flow conditions for the occurrence of cyclic flow patterns are summarized in Table 3, for the half-round circular weirs Type I and II. (With the circular weir Type III, the maximum discharge limitations prevented the occurrence of flow conditions for which the occurrence of cyclic flow patterns would be expected.) With the half-round circular weir Type I, the observations showed two ranges of discharge conditions during which a cyclic behaviour was observed. The periods of cyclic pattern were typically between 3 and 10 min, although some unusually wider range of periods, from 60 s to 12 min could be observed. With the larger half-round circular weir Type II, the data showed a marked difference between experiments conducted with increasing or decreasing discharges (Table 3). Thus, the comparison between the two weir observations suggested that the cyclic flow pattern was not a Froude-scalable phenomenon.

In practice, the repeated nappe detachment/attachment, while the discharge was kept constant, generated intense transient pressure loads on the weir and loud noises. The cyclic processes would induce vibration and fatigue to the weir wall, possibly impacting

the structural stability of thin-walled weir structures, during high-intensity transients (Rockwell & Naudascher, 1978). More, the attachments/detachments were associated with changes in upstream and downstream water levels, for a given constant discharge. The former might induce seiching and sloshing in the upstream reservoir. The latter could cause sudden changes in instantaneous outflow discharges, associated with water surges travelling downstream.

In practice, the cyclic pattern could be eliminated by nappe ventilation, e.g. using splitters.

## 6. Flow properties and discharge coefficient

Quantitative observations were undertaken for a broad range of flow rates (Table 1), with both increasing and decreasing discharges. In the following graphical data presentations, the mean flow conditions corresponding to changes in flow patterns, with increasing discharge experiments, are reported in thick vertical lines.

The upstream water depth data and downstream water depth data (data not shown) indicated a pseudo-monotonic increase in water depths with increasing discharges, with relatively close qualitative and quantitative data for all half-round circular weir Types I, II and III (i.e.  $P/r = 25$  and  $B/r = 40$ ). Some data scatter was observed for intermediate flow conditions corresponding to cyclic flow patterns during long duration experiments. The downstream depth data tended to show more data spread and differences between the three weir configurations, because of some difference in downstream flow patterns, with comparatively larger shock waves and cross-waves on the larger weirs.

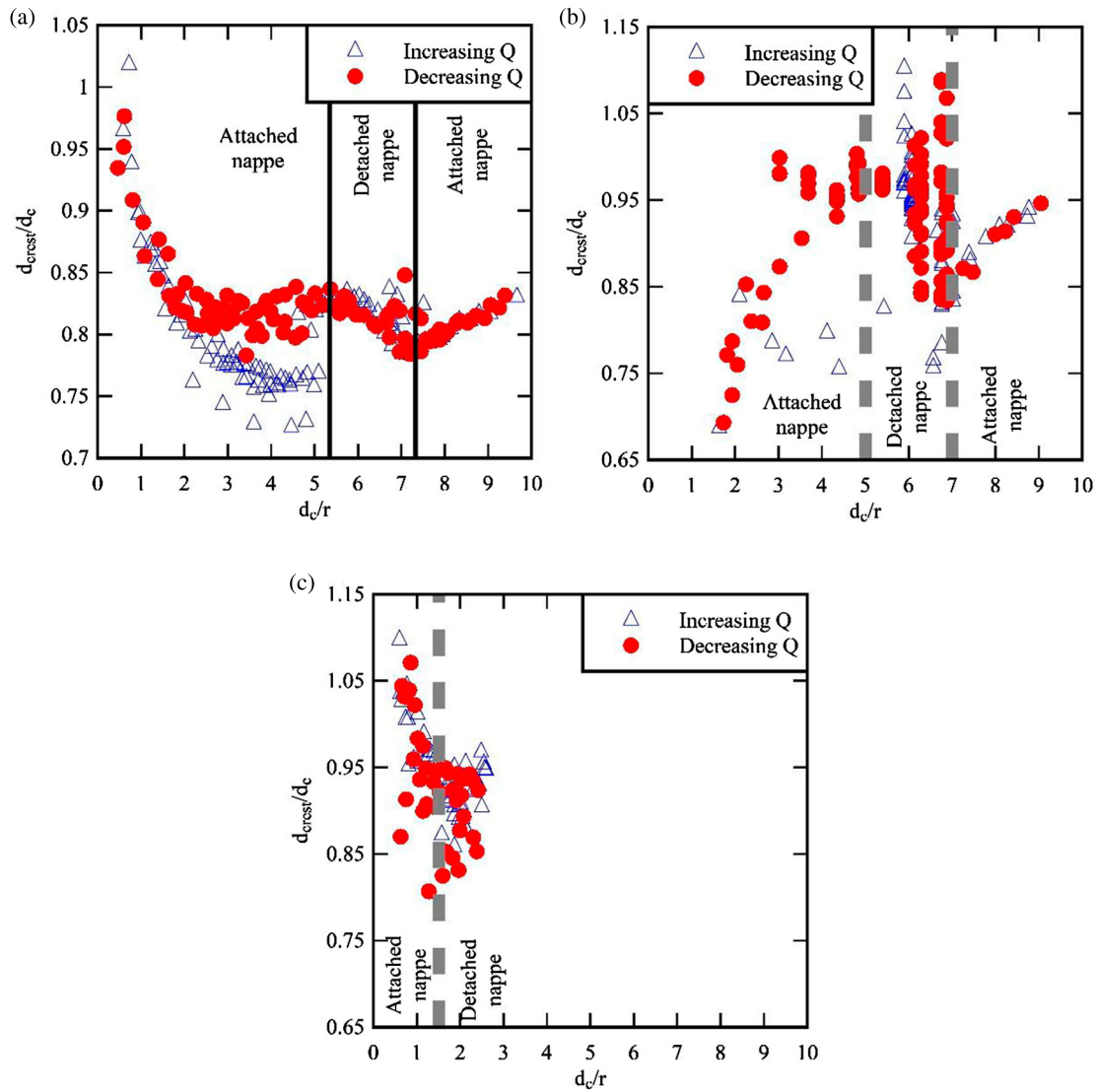


**Figure 6.** Dimensionless downstream water at the crest  $d_{crest}/d_c$  as a function of the dimensionless discharge  $d_c/r$  for (a) half-round circular weir Type I, (b) half-round circular weir Type II and (c) half-round circular weir Type III. The same legend and the same horizontal and vertical scales are used for all graphs. Note that half-round circular weir Type II data include instantaneous observations during cyclic nappe behaviour.

At the circular crest, the water depth  $d_{crest}$  differed from the ‘critical depth’  $d_c = (q^2/g)^{1/3}$  because of the non-hydrostatic pressure and non-uniform velocity distributions linked to the streamline patterns above the weir crest (Chanson, 2006, 2008; Fawer, 1937). The present experimental observations of water depth at the crest are reported in a dimensionless form in Figure 6, showing the ratio  $d_{crest}/d_c$  as a function of the dimensionless discharge  $d_c/r$ . Note that the data in Figure 6b encompassed instantaneous observations during cyclic flow patterns. The present data indicated some definite findings:

- a ratio  $d_{crest}/d_c$  mostly below unity, except at very low flow rate;
- some marked hysteresis, for all configurations, with different results for increasing and decreasing discharges;
- a lot of data scatter, especially among instantaneous observations during cyclic nappe behaviour;

- some major differences between the three circular weir configurations, despite the same dimensionless ratios  $P/r$  and  $B/r$ ;
- a series of complex unsteady experimental patterns which cannot be predicted by ideal fluid flow theory under steady conditions at a weir crest.

The vast majority of data yielded a ratio  $d_{crest}/d_c$  less than one (Figure 6). The minor exceptions were very low flow rate data and a few instantaneous observations during cyclic flow patterns. The result, i.e.  $d_{crest}/d_c < 1$ , was consistent with the ideal fluid flow theory, the observed streamline curvature and a flow net analysis (Castro-Orgaz & Hager, 2017; Rouse, 1932; Vallentine, 1969).

All the data showed some marked qualitative and quantitative differences between increasing and decreasing discharge experiments. Such a hysteresis implied that the observations of water depth at the crest

could not be used reliably to predict the discharges, in particular within  $2 < d_c/r < 8$ .

With the half-round circular weir Type II, a number of instantaneous observations of water depth at the crest, during cyclic flow patterns, were reported (Figure 6b). During these cyclic flow conditions with a constant discharge, the water depth data presented a large scatter. Overall, similar patterns were observed with half-round circular weir Types I and II. For completeness, during an experiment with  $d_c/r = 7.0$ , Chanson and Memory (2022, fig. 5) reported time-variations of instantaneous dimensionless water depth within  $0.92 < d_{crest}/d_c < 1.12$ .

The half-round circular weir Types I, II and III were designed with the same dimensionless ratios  $P/r$  and  $B/r$ , i.e. the half-round circular weir Types II and III being upscaled designed of half-round circular weir Type I. The present results were compared based upon

a combined Froude and Morton similitude and any difference, either qualitative or quantitative, would imply that the Froude similitude is not valid for the hydraulic modelling of half-round circular weirs and that the physical and numerical results cannot be extrapolated to prototype without scale effects. In Figure 6, the present data showed some major differences between the three half-round circular weir configurations. Qualitative differences included different flow conditions for the change in nappe attachment/detachment, as well as different trends in variations in  $d_{crest}/d_c$  with dimensionless flow rates  $d_c/r$ . Major quantitative differences, between half-round circular weir Types I and II, are seen for  $2 < d_c/r < 10$  between Figure 6a and b. While experimental errors, including operator errors, cannot be ignored, large differences between decreasing discharges were very likely linked to scaling issues of nappe ventilation and air entrainment at the lower nappe

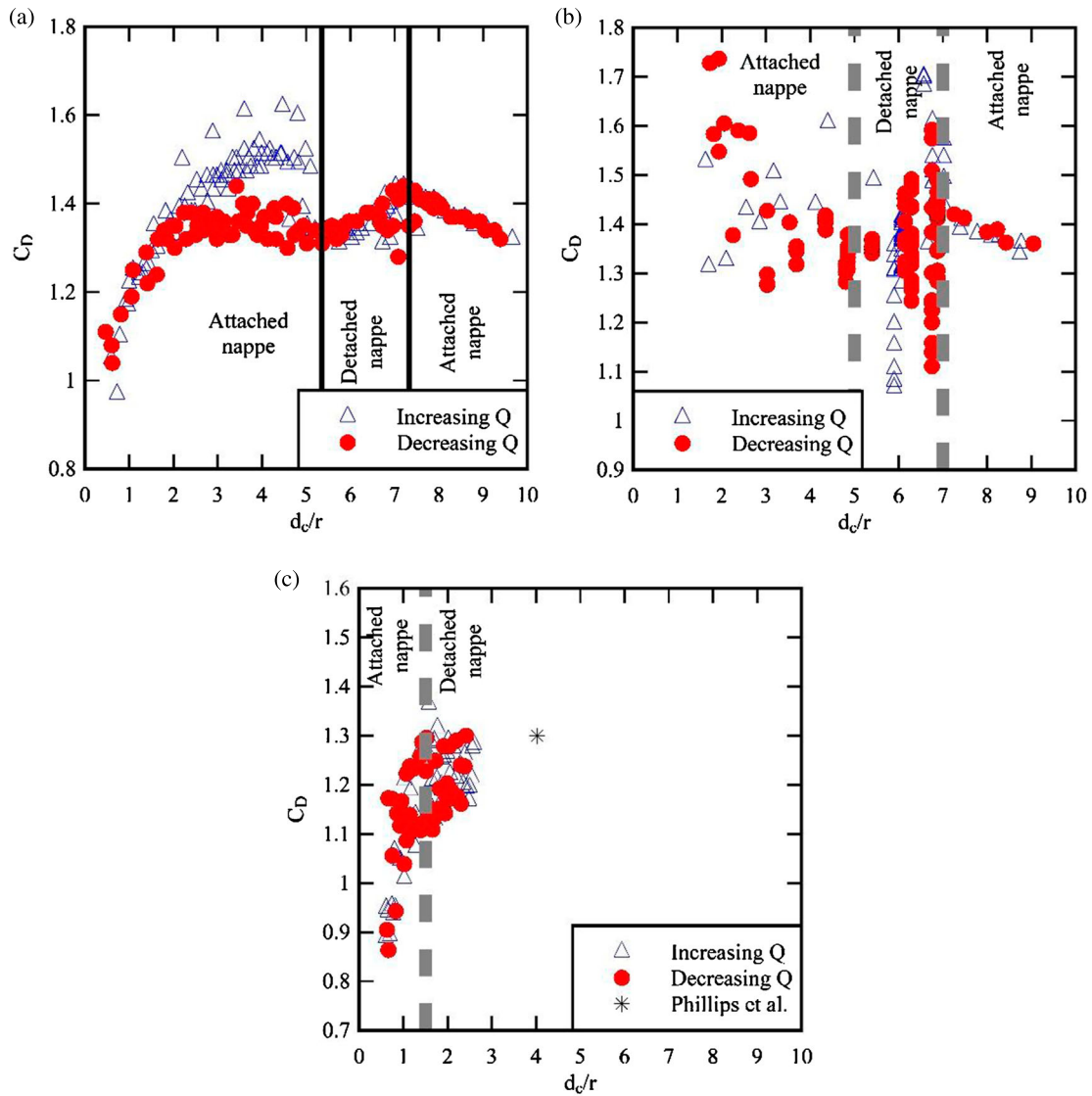


**Figure 7.** Dimensionless discharge coefficient  $C_D$  as a function of the dimensionless discharge  $d_c/r$  for (a) half-round circular weir Type I, (b) half-round circular weir Type II and (c) half-round circular weir Type III. The same legend and the same horizontal and vertical scales are used for all graphs. Note that half-round circular weir Type II data include instantaneous observations during cyclic nappe behaviour. Type III data are compared to conditions observed by Phillips et al. (2024) with ‘unstable partially aerated nappe’.

impingement. Indeed, it has well documented that ventilation and air bubble entrainment cannot be scaled with a Froude similitude (Chanson, 1997, 2013; Falvey, 1980; Rao & Kobus, 1974; Wood, 1991).

The rating curve of the weir crest is based upon the so-called 'weir equation' linking the volumetric discharge capacity to the upstream reservoir level (Equation 6). For the half-round circular weir configurations, the dimensionless discharge coefficient  $C_D$  data are reported in Figure 7. The comparative data showed a number of key outcomes:

- a discharge coefficient typically larger than unity, except at very low flow rate;

- a marked hysteresis with different results between increasing and decreasing discharge experiments;
- a significant data scatter, including for instantaneous observations during cyclic nappe behaviour;
- some differences between the three configurations despite identical dimensionless ratios  $P/r$  and  $B/r$ .

For all configurations, the dimensionless discharge coefficient  $C_D$  was greater than one, except at very low flow rates.  $C_D$  typically ranged from 1.1 to 1.7 (Figure 7). However, the data showed some marked differences between experiments with increasing and decreasing discharges. The observed hysteresis was directly associated with the lack of ventilation of the

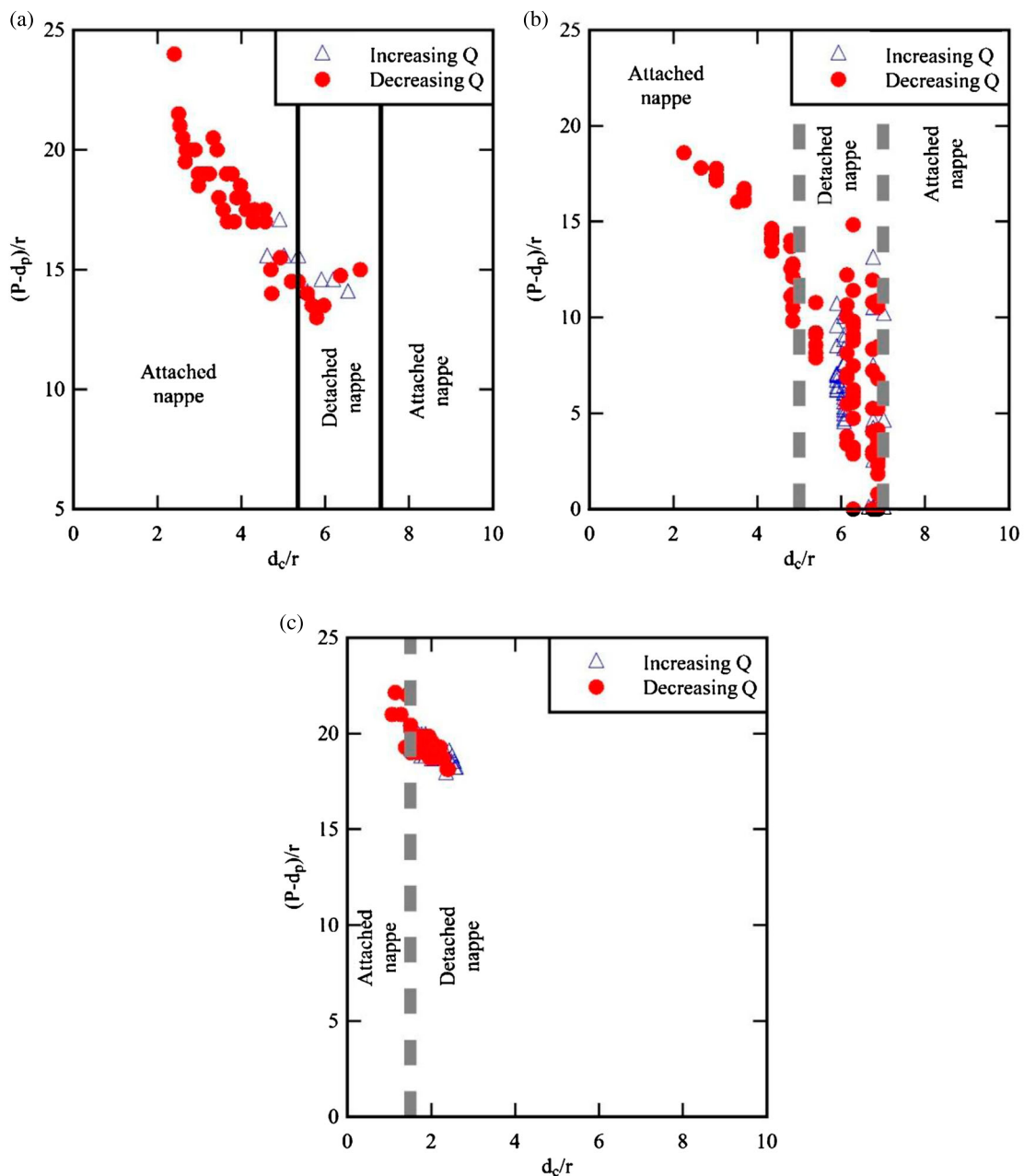


**Figure 8.** Dimensionless vertical height of air cavity  $(P-d_p)/r$  as a function of the dimensionless discharge  $d_c/r$  for (a) half-round circular weir Type I, (b) half-round circular weir Type II and (c) half-round circular weir Type III. The same legend and the same horizontal and vertical scales are used for all graphs. Note that half-round circular weir Type II data include instantaneous observations during cyclic nappe behaviour.

half-round circular weir configuration. The hysteresis implied that the rating curve of the circular weir would be nonlinear and unreliable for  $2 < d_c/r < 10$ , with different discharge predictions between increasing and decreasing discharge situations.

During cyclic flow patterns, the present observations showed large fluctuations, hence scatter, in terms of the discharge coefficient (Figures 5 and 7). The practical implications are not trivial because the cyclic processes are associated with sudden changes in overflow discharges that may induce vibrations to the weir and impact on its structural stability, while the oscillations of the trapped air volume trapped might cause adverse resonance effects, including horizontal banding and low frequency aero-acoustic noise.

Finally, the comparison between the three weir configurations datasets showed both qualitative and quantitative differences. The result implied that the dimensionless discharge coefficient could not extrapolated to prototype without significant scale effects.

## 7. Discussion

### 7.1. Air cavity features

For a range of intermediate flows, a well-defined air cavity formed below the detached nappe, and a pool of recirculating water developed underneath the air cavity (Figure 3a (middle)). The vertical height of the air cavity and the distance between the vertical weir wall

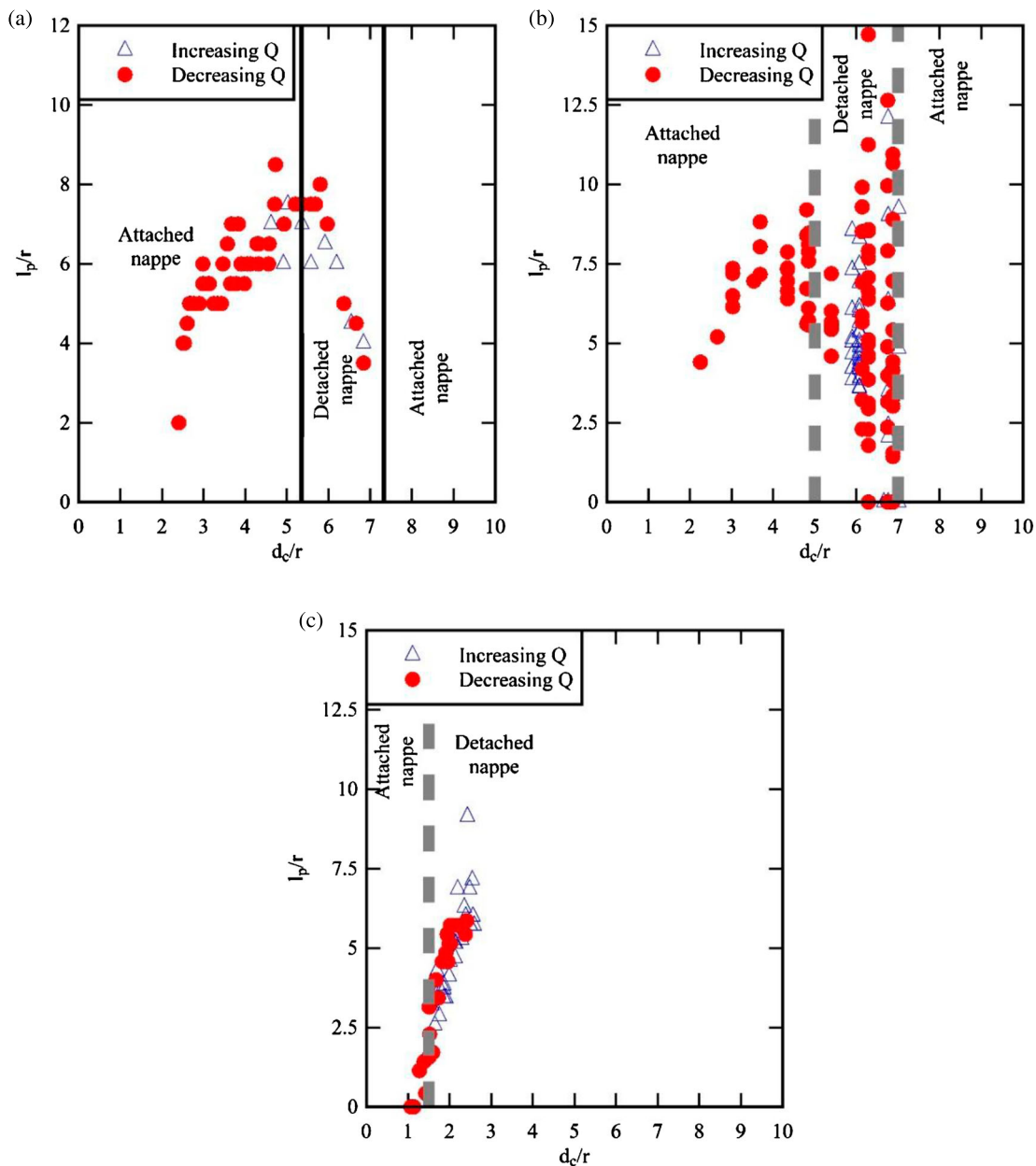


**Figure 9.** Dimensionless horizontal distance between weir wall and impingement perimeter of lower nappe  $l_p/r$  as a function of the dimensionless discharge  $d_c/r$  for (a) half-round circular weir Type I, (b) half-round circular weir Type II and (c) half-round circular weir Type III. The same legend and the same horizontal and vertical scales are used for all graphs. Note that half-round circular weir Type II data include instantaneous observations during cyclic nappe behaviour.

and the impingement perimeter of lower nappe were carefully documented. The results are reported in Figures 8 and 9 respectively. In Figures 8b and 9b, the data include instantaneous observations during cyclic nappe behaviour.

The data illustrated the wide range of air cavity dimensions during cyclic nappe flow conditions. These includes partial air cavity collapse as well as complete air cavity disappearance.

## 7.2. Upscaling limitations

The cyclic behaviour of the overflow nappe was caused by the lack of ventilation. For a half-round smooth circular weir in a rectangular channel in the absence of ventilation, a simple dimensional analysis yielded Equation (2), which was developed for steady flow conditions. The present experiments showed that the changes in flow regimes did not fulfil a Froude similarity, whether with increasing or decreasing discharges (Table 2). Moreover, Equation (2) did not account for nappe instabilities, and transient flow condition and cyclic flow instabilities which seemed to be non-Froude-scalable phenomena (Kolkman, 1972; Petrikat, 1978). For a half-round circular weir overflow, using the same fluids in model and prototype, the simplistic dimensionless Equation (5) would become:

$$C_D, \frac{d_{crest}}{r}, \dots = F_3 \left( \frac{H_1 - P}{r}, \text{Re}, t \times \sqrt{\frac{g}{r}} \right) \text{ Unsteady flow} \quad (7)$$

with  $t$  the time. While the above equation includes an additional independent parameter, i.e. the dimensionless time, the number of dependent variables would increase as well, with a number of relevant timescales relevant to air cavity fluctuations, fluid–structure interactions, etc.

The present observations suggested that the nappe reattachment and disappearance of air cavity was linked to some air bubble entrainment at the lower nappe impingement. The literature has long shown that air entrainment at hydraulics structures cannot be upscaled based upon a Froude similarity (Chanson, 1997; Rao & Kobus, 1974; Wood, 1991). At the same time, the nappe detachment and formation of air cavity was caused by the turbulent interactions between the contracted nappe and sidewalls. The associated viscous effects should be modelled based upon a Reynolds similitude and the results based upon a Froude similitude are unlikely to be upscaled without significant scale effects.

## 8. Conclusion

The half-round circular weir is a seminal weir crest configuration. At relatively small discharges, the flow

properties can be analysed theoretically based upon the ideal fluid flow theory of irrotational flow motion, flows, i.e. for  $d_c/r < 1$  to 1.2. At larger flow rates, a large amount of scatter and instabilities may be observed. Detailed investigations herein showed that the absence of ventilation caused some hysteresis and nonlinearities of the rating curve, and a detailed physical investigation of half-round circular weir overflow was conducted at three geometric scales for  $P/r = 25$  and  $B/r = 40$ . Three basic flow patterns were observed: an attached nappe with marked streamline curvature at low flow rates, a detached nappe with an air cavity underneath for a range of intermediate discharges, and a reattached nappe with some separation at large flow rates. The flow conditions for the change in flow patterns did not scale according to a Froude similitude. Some cyclic flow patterns were seen for a constant discharge, within a range of intermediate flow rates, for all the setups. The nonlinearities were caused by the lack of ventilation. The quantitative measurements indicated some hysteresis, with different results for increasing and decreasing discharge experimental conditions. Quantitative differences were also reported between the three setups, emphasizing the limitations and inadequacy of the Froude similitude at the toe of the weir.

In summary, the present research illustrated the physical complexity of the fluid dynamic patterns above a very simple weir crest geometry, with the occurrence of nonlinear flow features. The present application highlighted some major challenge in upscaling complex transient flows, including complex flow conditions during which the discharge was kept constant. The presence of hydrodynamic instabilities emphasized the importance of the quality of experimental setup and expertise of the individual experimentalists. In terms of engineering applications, the lack of ventilation was identified as a primary cause of instabilities. It led to unstable flow patterns observed in the Prado Dam spillway model with its nonlinear weir design. Other relevant engineering designs include lateral spillways equipped with half-round circular crest where no ventilation is commonly provided (e.g. Figure 1). Physically, nappe ventilation could be provided by some air conduit feeding the downstream wall of the weir, as well as nappe splitters installed along the crest and next to the sidewalls.

## Acknowledgements

The author would like to thank Professor Oscar Castro-Orgaz (University of Cordoba, Spain) and Professor Mohammad Ali Banihashemi (University of Tehran, Iran) for their helpful suggestions. He thanks his students, Chuyang Cai, Simeon Gover, Oscar Memory, and Zhengyi Zhang (in alphabetical order), for some data collection. He thanks further Professor A.S. Ramamurthy (Concordia University, Canada) for providing the original data of his former PhD student (Vo 1992), Ms Ya-Hui (Karen) Chou (Brisbane, Australia) for her help

with many field visits. The author acknowledges the technical assistance of Jason Van Der Gevel and Stewart Matthews (The University of Queensland, Australia).

## Disclosure statement

No potential conflict of interest was reported by the author(s).

## Data availability statement

All data, or models that support the findings of this study are available from the corresponding author upon reasonable request.

## Notation

$B$	channel width (m)
$C_D$	dimensionless discharge coefficient (–)
$d_c$	critical flow depth (m)
$d_{crest}$	water depth at the crest (m)
$d_p$	height of pool of recirculation water below the air cavity (m)
$g$	gravity acceleration ( $\text{m s}^{-2}$ ): $g = 9.794 \text{ m s}^{-2}$ in Brisbane, Australia
$H_1$	upstream total head (m)
$k_S$	equivalent sand roughness height (m)
$l_p$	air cavity length at lower nappe's impingement toe, i.e. horizontal distance between weir wall and impingement perimeter of lower nappe (m)
Mo	Morton number (–)
$P$	weir height (m)
$Q$	water discharge ( $\text{m}^3 \text{ s}^{-1}$ )
$q$	water discharge per unit width ( $\text{m}^2 \text{ s}^{-1}$ ): $q = Q/B$
Re	Reynolds number (–)
$r$	radius of curvature (m)
$x_1$	longitudinal location of the circular weir measured from the upstream end of the glass side-walled flume (m)
$\mu$	dynamic viscosity of water (Pa s)
$\theta$	angle between invert and horizontal
$\rho$	water density ( $\text{kg m}^{-3}$ )
$\sigma$	surface tension between air and water ( $\text{N m}^{-1}$ )
$c$	critical flow conditions
<i>Subscript</i>	
crest	crest flow conditions
1	upstream flow properties

## ORCID

Hubert Chanson  <http://orcid.org/0000-0002-2016-9650>

## References

- Ackers, P., White, W. R., Perkins, J. A., & Harrison, A. J. M. (1978). *Weirs and flumes for flow measurement*. John Wiley.
- Anderson, A., & Tullis, B. P. (2018). Finite crest length weir nappe oscillation. *Journal of Hydraulic Engineering, ASCE*, 144(6), Paper 04018020, 9 pages. doi:10.1061/(ASCE)HY.1943-7900.0001461
- Bertola, J., Wang, H., & Chanson, H. (2018). Air bubble entrainment, breakup and interplay in vertical plunging jets. *Journal of Fluids Engineering, ASME*, 140(9), Paper 091301, 13 pages. doi:10.1115/1.4039715
- Bertrand, J. (1878). Sur l'homogénéité dans les formules de physique. *Comptes Rendus*, 86(15), 916–920.
- Bin, A. K. (1993). Gas entrainment by plunging liquid jets. *Chemical Engineering Science*, 48(21), 3585–3630. doi:10.1016/0009-2509(93)81019-R
- Bos, M. G. (1976). *Discharge measurement structures*. Publication No. 161. Delft, The Netherlands: Delft Hydraulic Laboratory.
- Brattberg, T., & Chanson, H. (1998). Air entrapment and air bubble dispersion at two-dimensional plunging water jets. *Chemical Engineering Science*, 53(24), 4113–4127. doi:10.1016/S0009-2509(98)80004-3
- Buckingham, E. (1914). On physically similar systems; illustrations of the use of dimensional equations. *Physical Review*, 4(4), 345–376. doi:10.1103/PhysRev.4.345
- Casperson, L. W. (1993). Fluttering fountains. *Journal of Sound and Vibration*, 162(2), 251–262. doi:10.1006/jsvi.1993.1117
- Castro-Organ, O., & Hager, W. H. (2017). Non-hydrostatic free surface flows. In Holger Steeb, (Ed.), *Advances in geophysical and environmental mechanics and mathematics*. Springer. 696 pp.
- Chanson, H. (1997). *Air bubble entrainment in free-surface turbulent shear flows*. Academic Press.
- Chanson, H. (2004). *The hydraulics of open channel flow: An introduction* (2nd ed.). Butterworth-Heinemann.
- Chanson, H. (2006). Minimum specific energy and critical flow conditions in open channels. *Journal of Irrigation and Drainage Engineering, ASCE*, 132(5), 498–502. doi:10.1061/(ASCE)0733-9437(2006)132:5(498)
- Chanson, H. (2008). Minimum specific energy and critical flow conditions in open channels – closure. *Journal of Irrigation and Drainage Engineering, ASCE*, 134(6), 883–887. doi:10.1061/(ASCE)0733-9437(2008)134:6(883)
- Chanson, H. (2013). Hydraulics of aerated flows: Qui pro quo? *Journal of Hydraulic Research, IAHR*, 51(3), 223–243. doi:10.1080/00221686.2013.795917
- Chanson, H. (2020). Half-round circular crested weir: On hysteresis, instabilities and head-discharge relationship. *Journal of Irrigation and Drainage Engineering, ASCE*, 146(6), Paper 04020008. doi:10.1061/(ASCE)IR.1943-4774.0001473
- Chanson, H. (2024). *Hydraulic modelling of half-round circular weirs: Scaling considerations, non-linearities, instabilities, ventilation*. Hydraulic Model Report No. CH126/24. Brisbane, Australia: School of Civil Engineering, The University of Queensland. doi:10.14264/13436ec
- Chanson, H., & Memory, O. (2022, November 30-2 December). Hysteresis, non-linearity and instabilities on circular crested weir. In *Proceedings of 30th Hydrology and Water Resources Symposium HWRS2022, Brisbane, Australia*, 30 November-2 December (pp. 1116–1124). Published by Engineers Australia, Brisbane, Australia, Paper 156.
- Chanson, H., & Montes, J. S. (1998). Overflow characteristics of circular weirs: Effect of inflow conditions. *Journal of Irrigation and Drainage Engineering, ASCE*, 124(3), 152–162. doi:10.1061/(ASCE)0733-9437(1998)124:3(152)
- Falvey, H. T. (1980). Air-water flow in hydraulic structures. *USBR Engineering Monograph*, No. 41. Denver, Colorado, USA.
- Fawer, C. (1937). *Etude de Quelques Ecoulements Permanents à Filets Courbes. (Study of some steady flows with curved streamlines)*. Thesis. Imprimerie La Concorde.

- Foss, J. F., Panton, R., & Yarin, A. (2007). Nondimensional representation of the boundary-value problem. In C. Tropea, A. L. Yarin, & J. F. Foss (Eds.), *Springer handbook of experimental fluid mechanics* (pp. 33–82). Springer.
- Hager, W. H. (1992). Spillways, shockwaves and air entrainment – Review and recommendations. *ICOLD Bulletin*, No. 81, Jan. 117 pages.
- Ippen, A. T., & Harleman, R. F. (1956). Verification of theory for oblique standing waves. *Transactions, ASCE*, 121(1), 678–694. doi:10.1061/TACEAT.0007331
- Kobus, H. (1984, September 3–6). Local air entrainment and detrainment. In H. Kobus (Ed.), *Proceedings International Symposium on Scale Effects in Modelling Hydraulic Structures* (pp. Paper 4.10, 10 pages). Esslingen, Germany: IAHR.
- Kolkman, P. A. (1972). The necessity of allowing for the Reech-Froude condition in the similarity of turbulent hydro-elastic phenomena. *Journal of Hydraulic Research, IAHR*, 10(3), 113–125. doi:10.1080/00221687209500022
- Liggett, J. A. (1994). *Fluid mechanics*. McGraw-Hill.
- Matthew, G. D. (1963, August). On the influence of curvature, surface tension and viscosity on flow over round-crested weirs. *Proceedings of the Institution of Civil Engineers London*, 25, 511–524.
- MWSDB. (1980). Investigation into spillway discharge Noise at Avon Dam. *ANCOLD Bulletin*, (57), 31–36.
- Novak, P., & Cabelka, J. (1981). *Models in hydraulic engineering. Physical principles and design applications*. Pitman Publ.
- Pariset, E. (1955, August 31 - September 6). Etude sur la Vibration des lames Déversantes. ('Study of the vibration of free-falling nappes.'). In *Proc. 6th IAHR Congress* (Vol. 3, paper C21, pp. 1–15). The Hague, The Netherlands.
- Petrikat, K. (1958, February). Vibration tests on weirs and bottom gates. *Water Power*, 10, 52–57.
- Petrikat, K. (1978). Model tests on weirs, bottom outlet gates, lock gates and harbours moles. *M.A.N. Technical Bulletin*, Nurnberg, Germany, 36 pages.
- Phillips, M. A., Crookston, B. M., & Allen, J. (2024, June 17–19). Hydrodynamic pressures on high head – high labyrinth weir walls with considerations for weir wall structural loading – A case study – Prado Dam spillway. In R. M. Boes, I. Albayrak, S. Felder, B. Crookston, & V. Heller (Eds.), *Proceedings of the 10th International Symposium on Hydraulic Structures 2024 – 10th ISHS* (pp. 326–335). Zurich, Switzerland: ETH Zurich.
- Rao, N. S. L., & Kobus, H. E. (1974). Characteristics of self-aerated free-surface flows. In *Water and Waste Water/Current Research and Practice* (Vol. 10, 224 pages). Eric Schmidt Verlag.
- Ramamurthy, A. S., & Vo, N. D. (1993). Characteristics of circular-crested weir. *Journal of Hydraulic Engineering, ASCE*, 119(9), 1055–1062. doi:10.1061/(ASCE)0733-9429(1993)119:9(1055)
- Rockwell, D., & Naudascher, E. (1978). Review – self-sustaining oscillations of flow past cavities. *Journal of Fluids Engineering, Transactions ASME*, 100(2), 152–165. doi:10.1115/1.3448624
- Rouse, H. (1932). *The distribution of hydraulic energy in weir flow with relation to spillway design* [M.Sc. thesis]. Dept. of Civil Engineering, M.I.T.
- Tullis, B. P., Crookston, B. M., & Bung, D. B. (2018). Weir head-discharge relationships: A multilab exercise. *Call-for-Participation*, IAHR Hydraulic Structures Technical Committee, 2 pages.
- Tullis, B. P., Crookston, B. M., & Bung, D. B. (2019, September 1–6). Weir head-discharge relationships: A multilab exercise. In L. Calvo (Ed.), *Proc. 38th IAHR World Congress, Panama City*, 1–6 Sept. (pp. 486–500). IAHR Publication. doi:10.3850/38WC092019-0806.
- Vallentine, H. R. (1969). *Applied hydrodynamics* (SI edition). Butterworths.
- Vaschy, A. (1892). Sur les lois de similitude en physique. *Annales Télégraphiques*, 19 (Tome XI), 25–28.
- Wood, I. R. (1991). Air entrainment in free-surface flows. In *Iahr hydraulic structures design manual No. 4* (149 pages). Rotterdam, The Netherlands: Hydraulic Design Considerations, Balkema Publ.

## Appendix A. Movies of half-round circular weir overflow (Digital Appendix)

New physical experiments were undertaken in relatively large facilities with very smooth inflow conditions. The half-round circular weirs were installed perpendicular to the flow direction, sealed with silicone on the sides and bottom. Video movies were recorded during some experiments, while the discharge was kept constant. Their description and the corresponding flow conditions are listed in Table A1. The movies can be viewed in the online supplemental data for this paper.

**Table A1.** List of digital video movies and flow conditions.

Movie filename	$P$ (m)	$r$ (m)	$B$ (m)	$d_c/r$	Camera	Description
CIMG5661.mov	0.250	0.010	0.40	4.8	Casio™ EX-10 Exilim	Attached nappe, HD movie [30 fps] – Unventilated experiment which lasted 4–5 min. before apparition of air cavity with loud noise
IMG_E3223.mov	0.3125	0.0125	0.50	6.66	Apple™ iPhone XI	Cyclic flow pattern from attached to fully-detached nappe – 1080 px [30 fps]
IMG_E3227.mov				6.66	Apple™ iPhone XI	Cyclic flow pattern from attached to fully-detached nappe – 1080 px [30 fps]

Notes:  $B$ : channel breadth;  $d_c$ : critical flow depth ( $d_c = (q^2/(g))^{1/3}$ );  $P$ : weir height;  $Q$ : discharge;  $r$ : radius of curvature of crest.